# DESIGN AND CONSTRUCTION OF A DUAL OPTICAL TWEEZER

**A Thesis**

submitted to
Indian Institute of Science Education and Research Pune
in partial fulfillment of the requirements for the
BS-MS Dual Degree Programme

by

Jithin K


Indian Institute of Science Education and Research Pune
Dr. Homi Bhabha Road,
Pashan, Pune 411008, INDIA.

March, 2018

Supervisor: Dr. Umakant D Rapol

# Certificate

This is to certify that this dissertation entitled **"Design and construction of a dual optical tweezer"** towards the partial fulfillment of the BS-MS dual degree programme at the Indian Institute of Science Education and Research, Pune represents study/work carried out by **Jithin K** at **Indian Institute of Science Education and Research** under the supervision of **Dr. Umakant D Rapol**, Associate Professor, Department of Physics, during the academic year 2017-2018.

Dr. Umakant D Rapol

March 30, 2018

Committee:

Dr. Umakant D Rapol

Dr. G V Pavan Kumar

To my **parents** and my **sister**

# Declaration

I hereby declare that the matter embodied in the report entitled **"Design and construction of a dual optical tweezer"** are the results of the work carried out by me at the **Department of Physics, Indian Institute of Science Education and Research, Pune** under the supervision of **Dr. Umakant D Rapol** and the same has not been submitted elsewhere for any other degree.

Jithin K

March 30, 2018

# Acknowledgments

First of all, I would like to thank my guide, Dr. Umakant D Rapol for giving me the opportunity to work in the Atomic Physics and Quantum Optics Laboratory. He has always been a motivation and inspiration for me. I also acknowledge my co-supervisor Dr. Shicprasad Patil and Thesis Advisory Committee (TAC) member Dr. G V Pavan Kumar for their valuable suggestions. I also thank Dr. Chaitanya Athale and his student Yash Jawale for all the discussions and our most anticipated collaboration. I extend my gratitude towards Dr. Ayan Banerjee from IISER Kolkata and his student Shuvojit Paul for helping me gain more knowledge on optical tweezer and giving me the opportunity to visit their lab. I thank Dr. Thomas Pucadyil for providing me with the microscopic beads during the early stages of the experiment.

I am grateful to all my senior lab mates Dr. Sunil Kumar, Sumit Sarkar, Chetan Vishwakarma, Gunjan Verma and Jay Mangaonkar. They helped me learn many things in the lab. Whenever I got stuck with the project, they helped me solve the issues. They made the lab so lively that it's my fortune to work with all of them.

I'm not sure whether words would be enough to thank my father, mother, and sister. They are my constant source of support. I am very happy to dedicate my thesis to them. I am pleased to thank all my friends especially Swathi, Swetha, and Athul.I have learned a lot of things from them. The love, concern, and encouragement that I received from them are limitless.

# Abstract

Optical tweezers are a powerful experimental tool in studying many exciting areas in physical and biological sciences. The ability to apply forces in pico-Newton scales make it a versatile tool in studying properties of colloids, molecular motors, and microrheology. Optical tweezers are built over inverted microscopes with high numerical aperture objectives. There are a plethora of optical tweezer systems that are being used worldwide. The applications of single, dual, multiple trap and holographic optical tweezers are never-ending, making this system a very versatile tool for physicists and biologists alike. In the duration of this Master's thesis, the construction and calibration of a single and dual optical tweezer are demonstrated. The setup underwent significant changes in comparison to the standard design which has given it more experimental freedom. The tweezer can provide trap stiffness in the range of 20 pN/m to 140 pN/m.

# Contents

# Chapter 1

# Introduction

The concept of light exerting forces dates back to $17^{th}$ century. It was in 1619 that Johannes Kepler [1] proposed the idea of radiation pressure, the pressure experienced by a surface exposed to electromagnetic radiation. He hypothesized that radiation pressure causes the comet's tail to point away from the sun. It is now known that, as a comet approaches the sun, trapped gases get released from the comet nucleus due to heat and the radiation pressure directs the gases away from the sun.

In 1861, James Clerk Maxwell provided the theoretical explanation of radiation pressure [2], claiming that light is electromagnetic radiation, it carries momentum and hence can exert a pressure on any surface. Pyotr Lebedov in 1901 [3] and Ernest Fox Nichols and Gordon Ferrie Hull in 1903 [4] experimentally demonstrated the effect of radiation pressure. Ernest Nichols and Gordon Hull used an apparatus known as Nichols radiometer which consisted of a depressurized glass jar with mirrors made of microscope cover-slips suspended inside. On illumination with an arc lamp, the mirrors were seen to rotate, proving the existence of radiation pressure.

The first use of radiation pressure in the context of optical tweezers was in 1970 by Arthur Ashkin [5], ten years after the invention of the laser by Theodore Harold Maiman [6]. On il-

lumination by laser light, he observed micron-sized latex beads getting attracted towards the beam axis and accelerated in the direction of propagation of laser light. By trapping beads with sizes ranging from 0.5 $\mu$m to 2.5 $\mu$m using counter-propagating continuous wave (CW) Argon laser light ($\lambda$ = 514.5 nm), he explained the phenomenon of radiation pressure in optical tweezers. With one of the counter-propagating beam blocked, particles accelerated in the direction of the other beam. The experiment by Ashkin became the very first experiment on optical tweezers which opened up a new era of micro-manipulation of particles using laser light.

Single-beam gradient force optical tweezer was first achieved in 1986 by Arthur Ashkin *et al.* [7]. Using highly focused laser light, they showed the presence of a backward force component, known as gradient force due to the axial intensity gradient which resulted in the trapping of micron-sized beads with the help of a single laser beam. With the advent of single-beam optical tweezers, it became possible to address many problems in both Physics and Biology. A year later, in 1987, optical tweezer found application in trapping and manipulation of bacteria and viruses [8]. The possibility of applying and measuring pico-Newton level forces in optical tweezers helped studying several interesting areas of science including molecular motors [9] and dynamics of colloidal systems [10].

One novel experiment that can be performed with the optical tweezer system is finding the directionality of cargo transport in mix-molecular motor assays by external forcing. The molecular motors like kinesin and dynein are proteins which transports cell cargos like viruses and endosomes on microtubules [11] by generating force [12]. The mechanism behind walking and force generation by motors are studied using optical tweezers for kinesin [13] and dynein [14]. When both kinesin and dynein molecular motors with opposite directionality are attached to a cell cargo, a tug-of-war [15] takes place between the two and reduction in force generated by kinesin is observed [16]. Many chemical regulatory pathways are known [17] to affect one of the motor types and thus leading to directional transport. We hypothesize periodic forcing based physical pathway which effects the motors and resolves the tug-of-war. The *in vivo* forcing can

arise due to the flows generated by actin polymerization and cytoplasmic streaming [18, 19]. To test this hypothesis, wave-like external force can be provided to a mix-molecular-motor assay using a modulated optical tweezer trap. The assay can be made by adhering both kinesin and dynein motors to a glass slide which result in microtubules that move in response to the force generated by molecular motors. The biotin functionalized microtubule can be anchored to streptavidin-coated microscopic beads [20] modulated using an optical tweezer trap. The net force due to the assay can be monitored which will give an insight into the reason behind the directionality in the transport.

In this thesis, we will discuss the design, construction, and characterization of both single and dual optical tweezer. The second chapter deals with the theoretical foundations related to optical tweezers. It includes the contribution of various forces towards optical trapping, the motional properties of the trapped bead, the theory behind trap calibration methods. The third chapter discusses the in-house construction of single and dual optical tweezer, different design considerations and construction of fluorescence microscope. Chapter four consists of the results obtained for both single and dual optical tweezer system followed by a small discussion and future plans in chapter five.

# Chapter 2

# Theory

This chapter deals with the basic principles behind an optical tweezer. It includes the description of optical trapping forces, theoretical model explaining the motion of a trapped particle and trap stiffness calibration methods.

## 2.1 Forces behind optical tweezer

The principle of optical tweezer is based on the foundation that light carries momentum. With the earlier experiments on radiation pressure being inferred from the wave nature of light, the development of quantum mechanics provided the particle description of light. The optical field can be described as a collection of such single 'photons' with each one of them carrying one quanta of energy. The force exerted by the light can be explained in terms of momentum transfer between the photon and the particle.

The momentum of a photon can be written as $p = \hbar k$ where $\hbar$ is the reduced Plank's constant and $k$ is the wave vector. According to Newton's second law of motion, the force experienced by an object is proportional to the net rate of change of momentum. This suggests that when a particle interacts with laser light via refraction and scattering, a change in the momentum of photons takes place which results in a force. This force can be decomposed into two kinds viz. scattering force and gradient force. Scattering force acts in the direction of propagation of light

and can be considered as light pushing the particle. Gradient force acts in the direction of the gradient of light intensity, with particle pulled towards the region of higher intensity. Finally, the particle gets trapped little downstream the propagation axis away from focus of laser light, where both the scattering and gradient force get balanced.

To provide a steep intensity gradient that helps in balancing the two forces, a high numerical aperture (N.A.) microscope objective [21] is used to focus the laser light to a diffraction-limited spot. Even though the main principle behind optical trapping is well known, a complete theoretical foundation needs more rigor. For this, two different approaches based on the size of the particle are considered. When the size of the particle is much smaller in comparison to the wavelength of laser light used, Rayleigh approximation is considered. Ray optics regime is used when the particle size is much larger than the laser wavelength. Both the approaches agree with the experimental observations.

### 2.1.1 The Rayleigh regime

In the regime $d << \lambda$, where $d$ is the diameter of the particle and $\lambda$ is the wavelength of the laser light, Rayleigh approximation is used to explain the forces [22]. The particles are considered as point dipoles, and the laser light as an inhomogeneous electric field.

Lorentz force on a single charge by an electromagnetic field is given by

$$\mathbf{F}_L = q\left(\mathbf{E} + \frac{d\mathbf{x}}{dt} \times \mathbf{B}\right) \tag{2.1}$$

This force can be calculated by considering the dipole as two different charges separated by an infinitesimal distance $\mathbf{x}_1 - \mathbf{x}_2$. Taking $\mathbf{E}_1$ and $\mathbf{E}_2$ as the electric field experienced by the two opposite charges, the equation 2.1 becomes

$$\mathbf{F} = q\left(\mathbf{E}_1(x,y,z) - \mathbf{E}_2(x,y,z) + \frac{d(\mathbf{x}_1 - \mathbf{x}_2)}{dt} \times \mathbf{B}\right) \tag{2.2}$$

$$\mathbf{F} = q\left(\mathbf{E}_1(x,y,z) + ((\mathbf{x}_1 - \mathbf{x}_2)\cdot\boldsymbol{\nabla})\mathbf{E} - \mathbf{E}_1(x,y,z) + \frac{d(\mathbf{x}_1 - \mathbf{x}_2)}{dt} \times \mathbf{B}\right) \tag{2.3}$$

simplifying the above expression, we get

$$\mathbf{F} = (\mathbf{p}\cdot\boldsymbol{\nabla})\mathbf{E} + \frac{d\mathbf{p}}{dt} \times \mathbf{B} \tag{2.4}$$

where $\mathbf{p} = q\mathbf{d}$ is the polarization of the dipole, $\mathbf{d}$ is the distance between the two charges. Assuming the induced dipole moment is proportional to the electric field

$$\mathbf{F} = \alpha\left((\mathbf{E}\cdot\boldsymbol{\nabla})\mathbf{E} + \frac{d\mathbf{E}}{dt} \times \mathbf{B}\right) \tag{2.5}$$

where, $\mathbf{p} = \alpha\mathbf{E}$; $\alpha$ being the electric polarizability.

We know,

$$(\mathbf{E}\cdot\boldsymbol{\nabla})\mathbf{E} = \boldsymbol{\nabla}\left(\frac{1}{2}\mathbf{E}^2\right) - \mathbf{E} \times (\boldsymbol{\nabla} \times \mathbf{E}) \tag{2.6}$$

using the above identity along with the Maxwell's equation $\boldsymbol{\nabla} \times \mathbf{E} = -\dfrac{\partial \mathbf{B}}{\partial t}$, the equation 2.5 can be rewritten as-

$$\mathbf{F} = \alpha\left(\frac{1}{2}\boldsymbol{\nabla}\mathbf{E}^2 + \frac{d}{dt}(\mathbf{E} \times \mathbf{B})\right) \tag{2.7}$$

The second term in the equation 2.7 is the derivative of the Poynting vector to a multiplicative constant. This can be averaged to zero since the Poynting vector refers to power per unit area passing through a surface and our sampling rate is much shorter when compared to the frequency of laser light. This gives

$$\mathbf{F}_{grad} = \alpha\frac{1}{2}\boldsymbol{\nabla}\mathbf{E}^2 = \frac{2\pi n_0 a^3}{c}\left(\frac{m^2 - 1}{m^2 + 2}\right)\boldsymbol{\nabla}\mathbf{I}(r) \tag{2.8}$$

where $n_0$ being the refractive index of the medium, $a$ is the radius of the particle and $m = \dfrac{n_1}{n_0}$ is the relative refractive index. The equation 2.8 suggests that the force on the particle is proportional to the intensity gradient when the particles are considered as point dipoles. Scattering force which arises from the absorption and subsequent re-emission of light by the

dipole can be calculated using Rayleigh approximation

$$\mathbf{F}_{scat} = \frac{8\pi n_0 k^4 a^6}{3c}\left(\frac{m^2-1}{m^2+2}\right)^2 I(r)\hat{\mathbf{z}} \tag{2.9}$$

The scattering force of the light pushes the dipole in the axial direction of trap whereas the gradient force tries to bring the dipole to the region of intensity maximum.

### 2.1.2 The ray optics regime

When $d >> \lambda$, ray optics regime is used to explain the forces [23]. A light beam can be decomposed into a collection of rays with each of them following the Snell's law and Fresnel's law. Fresnel's law tells that when a ray passes from one medium to another both reflection and refraction may occur. According to Snell's law, a ray of light gets bent when it travels from one medium to another. Consider a spherical particle in the path of collimated laser light. For simplicity, take only two rays of light. As seen in the figure 2.1, rays get refracted on entering and exiting the bead. Refraction changes the direction of light which changes the momentum associated with the light. Light experiences a force due to the momentum change, and by Newtons' third law, the bead will experience an equal and opposite force. The more intense ray 2 exerts more force on the bead than the less intense ray 1. As a result, a bead displaced from the beam center gets a pull towards the center, due to the so-called gradient force. When a bead is at the center of collimated laser light, as depicted in figure 2.1, both the rays will have equal intensity, and the net force will be in the direction of propagation of laser light.

As mentioned earlier stable trapping can be achieved using focused laser light. When displaced in axial direction, gradient force pulls the bead towards the region of maximum intensity. As shown in the figure 2.2, when a bead is displaced from the focus along the axial direction, gradient force due to the momentum change bring the bead back to the focus. The absorption and reflection of the light results in another force known as scattering force which pushes the bead in the axial direction. The push by the scattering force is compensated by the gradient

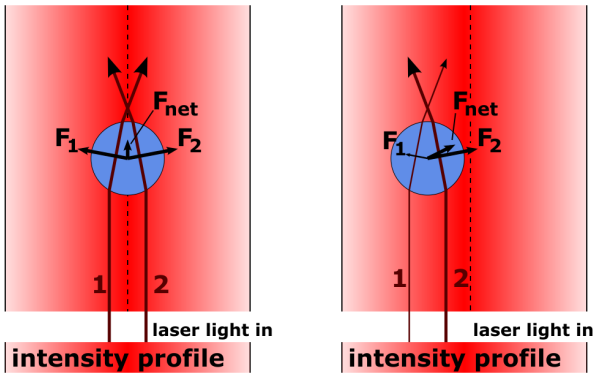


Figure 2.1: Ray optics explanation for bead in unfocused laser light [24]

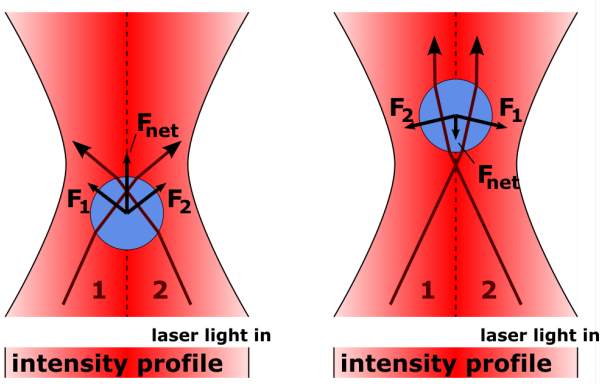


Figure 2.2: Ray optics explanation for bead in focused laser light [24]

force which pulls the bead towards the focus and bead finally gets trapped.

## 2.2 Brownian motion

When microscopic particles are suspended in a fluid, the particles undergo random movement due to the collision with neighboring molecules. This phenomenon known as Brownian motion was first observed by Robert Brown in the year 1827. He observed particles from pollen grains undergoing random motion when suspended in water. Similar kind of movement can be seen when microscopic beads are dispersed in water.

The theory behind Brownian motion was formulated by Albert Einstein in 1905 [25]. He gave

a relation between the macroscopic diffusion constant $D$ and the atomic parameters

$$D = \frac{RT}{N_A 6\pi\eta a} = \frac{k_B T}{6\pi\eta a} \tag{2.10}$$

where $N_A = 6.022 \times 10^{23}$ mol$^{-1}$ is the Avogadro number, $T$ is the temperature, $R = 8.314$ Jmol$^{-1}$K$^{-1}$ is gas constant, $\eta$ is the viscosity of the liquid, $a$ is the radius of the particle and $k_B = R/N_A$ is Boltzmann constant. According to Newton's first law of motion

$$\mathbf{F}(t) = m\frac{d\mathbf{v}(t)}{dt} \tag{2.11}$$

where $m$ is the mass of the particle, $\mathbf{v}(t)$ is the velocity of particle in the fluid, and $\mathbf{F}(t)$ is the total instantaneous force on particle. This force arises from the interaction of particle with the medium and consists of frictional force $-\gamma\mathbf{v}(t)$ and random force $\mathbf{F}_{random}(t)$ due to density fluctuations in the fluid. Substituting these two forces in 2.11 gives

$$m\frac{d\mathbf{v}(t)}{dt} = -\gamma\mathbf{v}(t) + \mathbf{F}_{random}(t) \tag{2.12}$$

The equation 2.12 is known as Langevin equation for a Brownian particle. Here $\gamma = 6\pi\eta a$ is the friction coefficient. The random force

$$\mathbf{F}_{random}(t) = (2k_B T\gamma)^{1/2}\boldsymbol{\zeta}(t) \tag{2.13}$$

is white noise [26] with amplitude $(2k_B T\gamma)^{1/2}$, $\boldsymbol{\zeta}(t)$ is a stochastic process with zero mean and delta function as its autocorrelation function i.e.

$$\langle\boldsymbol{\zeta}(t)\rangle = 0, \quad \langle\boldsymbol{\zeta}(t)\boldsymbol{\zeta}(t')\rangle = \delta(t-t') \tag{2.14}$$

Sustituting the value of $F_{random}(t)$ in 2.12 and restricting the motion in one dimension gives

$$m\frac{dv(t)}{dt} = -\gamma\frac{dx(t)}{dt} + (2k_B T\gamma)^{1/2}\zeta(t) \tag{2.15}$$

## 2.3 Optical tweezer as overdamped harmonic oscillator

Harmonic oscillator is a system where the particle experiences a restoring force which is linear and opposite to the displacement from its equilibrium position. The restoring force, $F_{rest}$ is given by,

$$F_{rest} = -kx \tag{2.16}$$

where $k$ is the spring constant of the system, $x$ is the displacement from equilibrium position. When $F_{rest}$ is the only force, then the system undergoes simple harmonic motion (SHM). When frictional force is present in the system, then the oscillator is said to be damped. Damping forces become significant when a system is immersed in a fluid and the general equation of motion of a viscously damped SHM is

$$m\ddot{x} + \gamma\dot{x} + kx = 0 \tag{2.17}$$

where $m\ddot{x}$ is the inertial force term, $\gamma\dot{x}$ is the viscous force term and $kx$ is the harmonic force term. In overdamped harmonic oscillator systems, the viscous term and harmonic force term dominates over the inertial term.

In optical tweezers, for small displacements from the equilibrium position, the gradient restoring force acting on the trapped bead is proportional to the displacement from the equilibrium position [21], $F_{trap} = -k_{trap}x$. The fluid surrounding the bead gives the viscous force, which is proportional to the velocity of the bead. Leonard S Ornstein and George E Uhlenbeck [27] studied the Brownian motion of particle under the influence of harmonic trap and is described using the following equation,

$$m\frac{dv(t)}{dt} = -\gamma\frac{dx(t)}{dt} - k_{trap}x + (2k_BT\gamma)^{1/2}\zeta(t) \tag{2.18}$$

The equation 2.18 above consists of all force terms present in an optical tweezer system. If the experimental timescale is far higher than $t_{inert}$, the characteristic timescale for loss of kinetic

energy though friction, then the inertial term has negligible effect. The typical value of $t_{inert} = m/\gamma$ is $10^3$ times lesser [28] than experimental time resolution. Hence the inertial force can be neglected when compared to the harmonic and viscous force, optical tweezer can be considered as an overdamped harmonic oscillator [29]. The inertial term can be dropped and equation 2.18 becomes

$$\gamma\frac{dx(t)}{dt} + k_{trap}x = (2k_BT\gamma)^{1/2}\zeta(t) \tag{2.19}$$

## 2.4 Stiffness calibration

The knowledge of trap stiffness is vital in characterizing the optical tweezer setup. Two major methods for finding the trap stiffness are power spectral density (PSD) method and equipartition method.

### 2.4.1 Power spectral density method

One of the most reliable method for finding the trap stiffness is PSD method. In this, the power spectrum of the Brownian motion of the trapped bead [28] is used to find the trap stiffness. The equation 2.19 describes the Brownian motion of a trapped bead in an overdamped system. Rewriting equation 2.19 gives

$$\gamma\frac{dx(t)}{dt} + k_{trap}x = (2k_BT\gamma)^{1/2}\zeta(t) \tag{2.20}$$

Power spectrum or power spectral density is the modulus square of the Fourier transform of a time series $x(t)$. The Fourier transform of $x(t)$ is

$$\tilde{x}(\omega) = \int_{-\infty}^{\infty} x(t)e^{i\omega t dt} \tag{2.21}$$

The first derivative of $\tilde{x}(\omega)$ will be

$$\frac{\partial\tilde{x}(\omega)}{\partial t} = \frac{\partial}{\partial t}\int_{-\infty}^{\infty} x(t)e^{i\omega t dt} = i\omega\tilde{x}(\omega) \tag{2.22}$$

The Fourier transform of equation 2.20 will be

$$i\omega\gamma\tilde{x}(\omega) + k\tilde{x}(\omega) = (2k_BT\gamma)^{1/2}\tilde{\zeta}(\omega) \tag{2.23}$$

where $\tilde{\zeta}(\omega)$ is the Fourier transform of $\zeta(t)$. Rewriting the equation 2.23 by keeping only $\tilde{x}(\omega)$ gives

$$\tilde{x}(\omega) = \frac{(2k_BT\gamma)^{1/2}\tilde{\zeta}(\omega)}{i\omega\gamma + k} \tag{2.24}$$

Power spectral density $S_x(\omega)$ can be obtained by multiplying equation 2.24 by its complex conjugate, ie $S_x(\omega) = \tilde{x}(\omega)\tilde{x}^*(\omega)$

$$\tilde{x}^*(\omega) = \frac{(2k_BT\gamma)^{1/2}\tilde{\zeta}^*(\omega)}{-i\omega\gamma + k} \tag{2.25}$$

$$S_x(\omega) = \frac{S_F(\omega)}{\omega^2\gamma^2 + k^2} = \frac{4\gamma k_BT}{\omega^2\gamma^2 + k^2} \tag{2.26}$$

here $S_F(\omega) = 4\gamma k_BT$ is the power spectral density of the random white noise [30]. Dividing by $\gamma$ and substituting $\omega = 2\pi f$ and corner frequency $f_c = k/2\pi\gamma$ in equation 2.26 gives

$$S_x(\omega) = \frac{4k_BT}{4\pi^2f^2 + 4\pi^2f_c^2} = \frac{k_BT}{\gamma\pi^2(f^2 + f_c^2)} \tag{2.27}$$

The PSD follows Lorentzian. Corner frequency divides the spectrum into two parts, for $f << f_c$ the power spectrum is constant which tells that the motion of the trapped bead is suppressed. For frequencies $f >> f_c$, bead undergoes free diffusion since power spectrum falls as $1/f^2$. Using the value of corner frequency, the trap stiffness $k_{trap} = 2\pi f_c\gamma$ can be obtained.

### 2.4.2 Equipartition method

Another method for finding the trap stiffness of an optical tweezer system is using Equipartition theorem [21]. Equipartition theorem tells that, at thermal equilibrium each degree of freedom contributes $\frac{1}{2}k_BT$ of energy to the total energy of the system. A trapped bead in an optical

tweezer system will have a harmonic potential energy of $\frac{1}{2}kx^2$. These can be related as,

$$\frac{1}{2}k_BT = \frac{1}{2}k\langle x\rangle^2 \tag{2.28}$$

where $\langle x\rangle^2$ is the time independent variance of the bead position from the trap center. Thus by measuring the positional variance of the trapped bead, the trap stiffness can be directly found out using the equation 2.28.

# Chapter 3

# Experimental details

The experimental section can be broadly divided into three parts. First one is the construction of a single optical tweezer system. The major components of an optical tweezer system include an inverted microscope, a high N.A. objective and a high power laser for trapping. Microscope lamp and a charged couple device (CCD) camera facilitate bead imaging. Trap stiffness calibration is achieved using a tracking laser, a quadrant photodiode (QPD) and a spectrum analyzer.

The second part of the experimental section deals with the construction of a dual optical tweezer system. Dual optical tweezer with independently steerable traps is derived from our single optical tweezer system. Third part consists of construction of a fluorescence microscope.

## 3.1 Construction of an optical tweezer

As mentioned earlier, an optical trap can be realized using a microscope, high power laser, and a high N.A. objective. An inverted microscope (Olympus, model number: IX71) with some modifications is used for the construction of optical tweezer. One major modification is the replacement of default microscope stage with an automated New Focus picomotor sample stage [31]. This sample stage is connected to a New Focus (model number: 9066M) stainless steel crossed roller translation stage using a right angle mount. The translation stage mounted on New Focus (model number: 9042M) baseplate can be attached to the microscope stage.

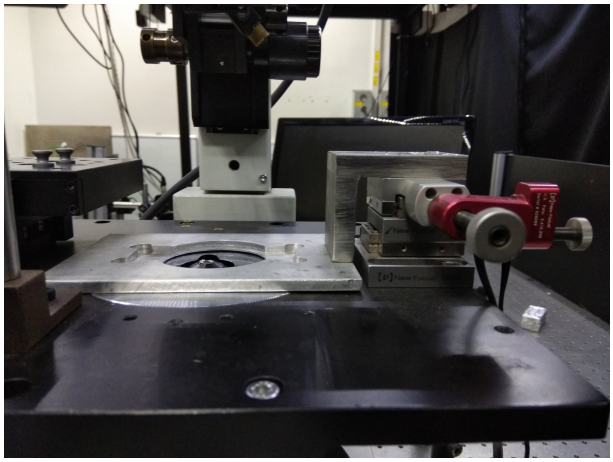

Figure 3.1: Translation stage assembly used in the optical tweezer system

Two New Focus piezoelectric actuators (US patent number 5,410,206) with a step size of 30 nm along with a New Focus motor joystick (model number: 8754) helps in achieving precise and controlled movement of the sample translation stage. An image of the translation assembly system used is given in figure 3.1.

As we have seen in the last section, the trap strength is dependent on the gradient of focused laser light, better trapping can be achieved using tighter focus. The numerical aperture of a microscope objective is the parameter which decides how tight a focus can be. The numerical aperture is defined as

$$N.A. = n\sin(\theta) \tag{3.1}$$

here $n$ is the refractive index of the objective immersion medium, $\theta$ is the half angular aperture. Higher N.A. implies higher $\theta$ and hence tighter focus. A water immersion (Olympus, model number: UPLSAPO 60XW, N.A. = 1.2) objective is used for the optical tweezer system.

The outermost rays emanating from the trapping laser contribute more towards the axial gradient force, and the central rays are responsible for the scattering force. Overfilling the entrance pupil of the objective by expanding the Gaussian trapping laser beam can increase the contribution of the outermost rays. This results in better axial gradient force and thereby improves the trap strength. In the present work, trapping is realized using a high power Infrared laser (Laser

Quantum, model: Ventus 1064, maximum output power = 3 W, $\lambda$ = 1064 nm). The $1/e^2$ beam diameter of trapping laser is 2.4 mm $\pm$ 0.2 mm, and the entrance pupil of the objective has a diameter of 8 mm. Two lenses in simple telescope configuration which gives a magnification ratio of $f_2/f_1$ can be used to expand the trapping laser light. Choosing $f_1$ = 50 mm and $f_2$ = 150 mm for lenses L1 and L2 gives a magnification factor of three and is used for overfilling the aperture. The figure 3.2 shows the optical layout of the single tweezer setup.

The laser light after the expansion is directed to the entrance port present at the bottom-back side of the inverted microscope with the help of two dielectric steering mirrors M1 and M2. In inverted microscopes, a dichroic mirror inside the microscope is used to direct the incident rays to the entrance pupil of the objective. The same dichroic mirror also helps to access the camera port on the bottom-left-hand side of the microscope. The thickness of the dichroic mirror caused multiple reflections, i.e., rays get reflected from both the front and back side of the dichroic mirror resulting in unwanted interference fringes causing major problems in bead movement detection. Bead movement is monitored using a tracking laser (Toptica Photonics, model: DL 100 pro design, maximum output power = 120 mW, $\lambda$ = 795 nm). The tracking laser is passed through an optical fiber for getting a relatively clean $TEM_{00}$ mode. A dielectric mirror M3, a polarizing beam splitter (PBS1) and two half-wave plates HWP1 and HWP2 helps in overlapping both the trapping and tracking laser light with maximum power.

The problems due to the dichroic mirror are solved by replacing it with a dielectric mirror (M5). The replacement caused the camera port unaccessible for imaging the bead. For imaging the beads, the same dichroic mirror (DM1) is placed before the entry port of the microscope in such a way that both trapping and tracking light gets transmitted through the dichroic mirror and reaches the objective. Imaging is achieved with the aid of a CCD camera (Cohu, model number: 4912 - 5000/0000) and a microscope lamp. In the inverted microscope setup, the microscope lamp illuminates the sample and passes through the 60X objective. This light gets reflected from M5 and reaches DM1. On reaching DM1, the light gets both reflected and trans-

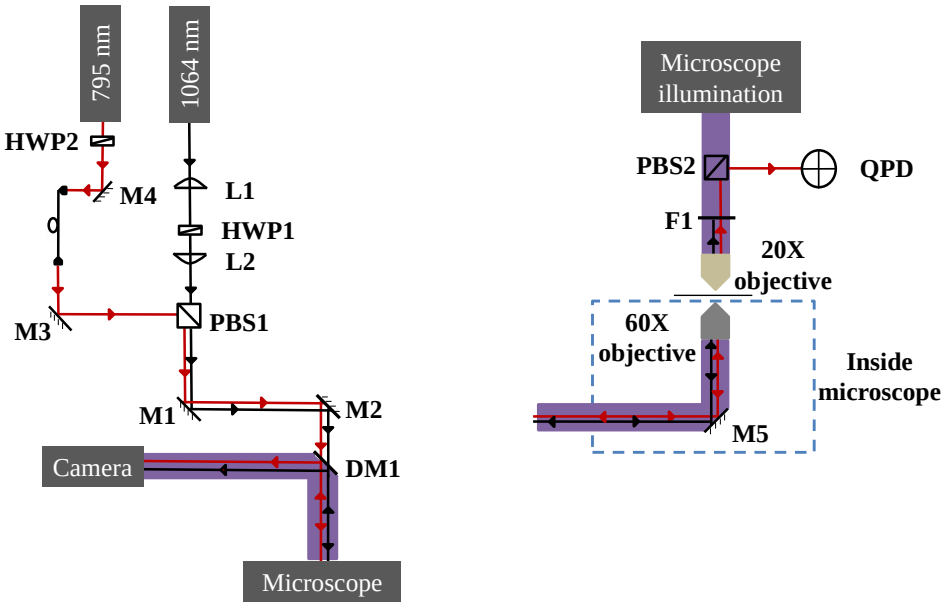


Figure 3.2: Optical layout of single optical tweezer

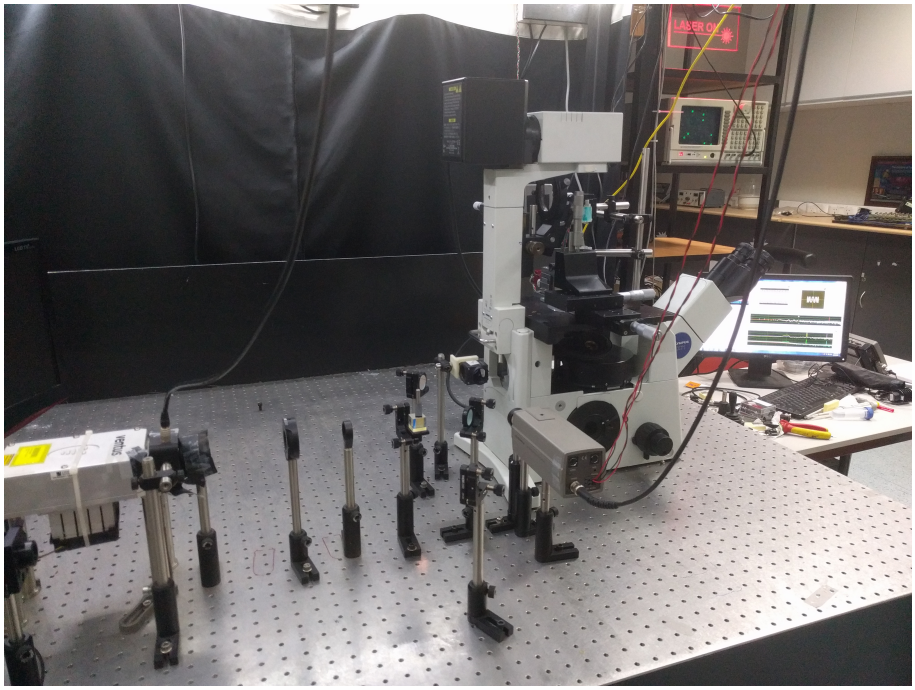

Figure 3.3: Single optical tweezer system

mitted. Since the transmission path is same as the laser light path, the CCD camera is placed in the reflection path. A lens L3 is placed in this path to converge maximum illumination light to the camera. The camera is connected to a TV monitor to view the beads.

## 3.2 Bead sample preparation and trapping

Bead sample preparation is an essential part in the optical tweezer. Beads of two different sizes are used.

1. 1 $\mu$m carboxylate modified polystyrene beads (Sigma Aldrich, model number: L4655)

2. 2 $\mu$m polystyrene beads (Bangs Laboratories, model number: NT17N)

The beads are diluted in distilled water using serial dilution method. 2 $\mu$L of bead stock solution is pipetted into an Eppendorf tube containing 1 mL of distilled water to form dilution mixture 1. 10 $\mu$L of dilution mixture 1 is pipetted into another Eppendorf containing 1 mL of distilled water to form dilution mixture 2. Dilution mixtures for both 1 $\mu$m and 2 $\mu$m beads are prepared. A dilution factor of 1:50,000 is achieved using this serial dilution technique. After each step, the dilution mixtures are sonicated for about 5 minutes, uniformly distributing the beads in the mixture.

The working distance of the 60X objective is 0.28 mm, which results in laser light getting focused within the normal microscope glass slide. Microscopic beads are successfully trapped by replacing the glass slide with rectangular cover glass (Blue star, dimensions: 24 mm $\times$ 60 mm). The rectangular cover glass is placed over the water immersion objective and 50 $\mu$L of dilution mixture 2 is drop-casted onto the rectangular cover glass. A square cover glass (Blue star, dimensions: 25 mm $\times$ 25 mm) is placed over the sample which results in a thin layer of sample ready for trapping.

The next step is to trap the microscopic beads. Once the sample is placed on the sample

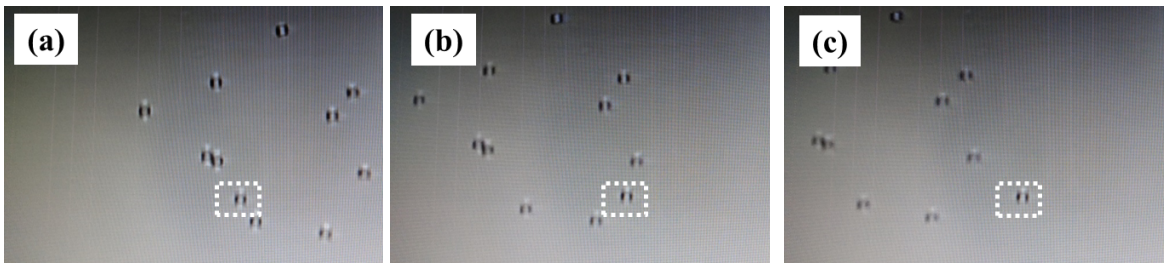


Figure 3.4: (a), (b), (c) shows the effect of translation of sample stage with the highlighted bead being trapped. On moving the stage towards left, the trapped bead stays intact while all other beads move along with the stage.

stage, microscope lamp is turned on illuminating the sample. Movement of the sample in the horizontal plane is achieved using the picomotor translation stage. The resolved image of beads can be obtained by coarse and fine adjustments of the microscope objective. A bead can be trapped by moving it towards the laser focus using the picomotor joystick and playing with the vertical adjustment of the objective.

## 3.3 Bead position detection and stiffness calculation

As mentioned earlier, bead movement is monitored using a tracking laser and a quadrant photodiode. The tracking laser light on illuminating a trapped bead gets scattered in all directions. The light scattered in the forward direction is used for monitoring the movement of the beads. The back-scattered light from the beads can be accessed only from the path where the camera is placed. But since rays get reflected from both the sides of the dichroic mirror in this path, the unwanted interference fringes as mentioned earlier causes problems in the detection. One more advantage of using forward scattered light is the possibility of three-dimensional particle tracking [32].

The forward scattered light is collected and directed to the quadrant photodiode. The forward scattered light can be collected using a converging lens, condenser of the microscope or by using another microscope objective. All the three schemes are tried in the optical tweezer system. Since a higher N.A. objective is used for trapping, the scattering of light happens at very large

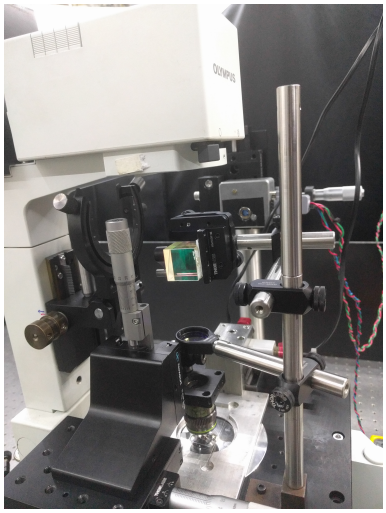

Figure 3.5: Trapped bead position detection scheme.

angles. Both the converging lens and condenser are not able to collect all the scattered light. An air immersion objective (Olympus, model: LUCPLFLN 20X, N.A. 0.45) mounted on an XYZ translator is used for collecting the forward scattered light.

The forward scattered light from a trapped bead contains the information about the position of the bead. The position and movement of a trapped bead are monitored using a quadrant photodiode (OSI Optoelectronics, model number: QD-50-0-SD). A QPD consists of four photodiode quadrants separated by a small gap. The forward scattered light is directed onto the QPD such that more intense bead shadow falls on the center of the QPD. The QPD along with its associated circuitry provides two difference signals and a sum signal. The sum signal is the amplified sum of the voltages of all the four quadrants. The difference signals are voltage signals which correspond to the relative intensity of the light detected by opposing pairs of quadrants. As seen in the figure 3.6, let us consider the four quadrants $Q_1$, $Q_2$, $Q_3$, $Q_4$ with voltages $V_1$, $V_2$, $V_3$, $V_4$ respectively. Then the difference signals are

$$V_X = (V_2 + V_3) - (V_1 + V_4) \tag{3.2}$$

$$V_Y = (V_1 + V_2) - (V_3 + V_4) \tag{3.3}$$

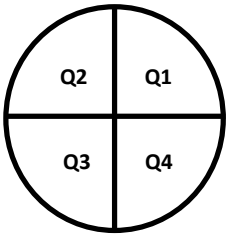


Figure 3.6: Illustration of a quadrant photodiode

where $V_X$ and $V_Y$ represents the X and Y voltages.

A polarizing beam splitter (PBS2) placed between the microscope lamp and the 20X objective allows reflection of tracking laser light along with transmission of microscope bright light. The QPD mounted on a XYZ translator is placed in this reflection path of tracking laser along with a filter (F1) which transmits only tracking laser light. The Brownian motion of a trapped bead will result in X and Y voltage signals which are linear to the position fluctuation of the bead. This information of the bead position is used to calculate the trap stiffness using PSD method. The voltage signal from the QPD is fed into a spectrum analyzer (Stanford Research Systems, model number: SR785). The spectrum analyzer, when used in FFT mode, gives the PSD of the trapped bead. From PSD, corner frequency and the trap stiffness can be found out.

## 3.4 Construction of dual optical tweezer

A dual optical tweezer consists of two optical traps where beads can be trapped simultaneously. An assembly of two polarizing beam splitters, two half-wave plates, two quarter-wave plates and two mirrors are used to derive dual trap from the single tweezer setup. The PBS1 overlaps both trapping and tracking light. The half wave plates HWP1 and HWP2 can be rotated in such a way that, transmitted and reflected light from PBS1 of both the trapping and tracking laser beams have separately equal power. The laser lights split into two paths viz path1 and path2 with overlapped trapping and tracking light in each path having polarizations perpendicular to each other. To achieve dual optical tweezing, two spatially separated light path needs to

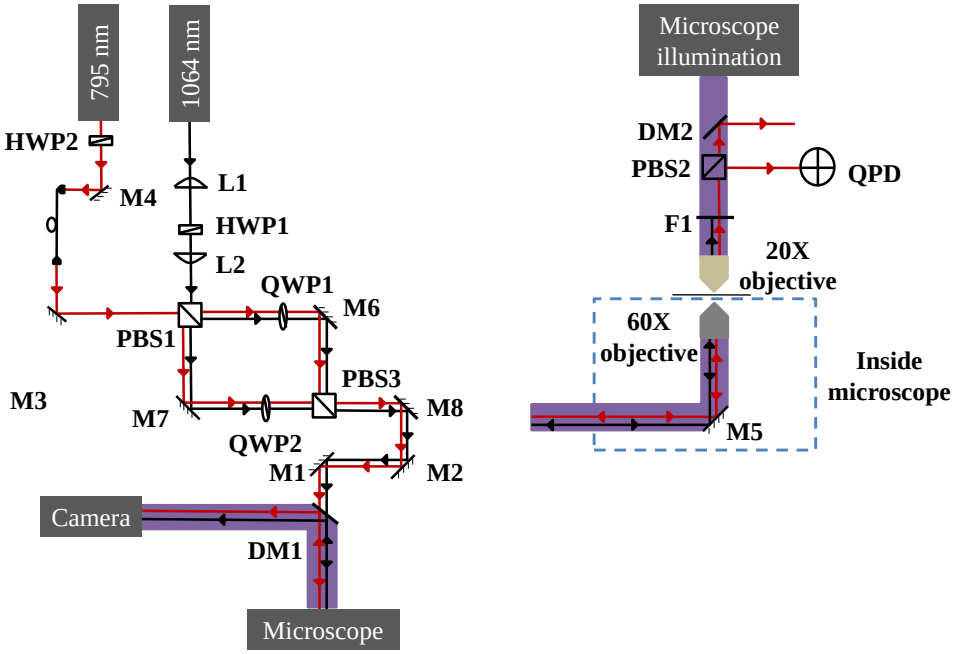


Figure 3.7: Dual tweezer optical layout

enter the entrance pupil of the water immersion objective simultaneously. The overlapped laser lights in each path are passed through quarter wave plates, QWP1 and QWP2 changing the plane polarized lights into spherically polarized lights. After reflection through the mirrors M6 and M7, the spherically polarized lights are passed through another polarizing beam splitter (PBS3). On passing through PBS3, the overlapped laser lights in each path will have both reflected and transmitted components with equal power. By moving the mirrors M6 and M7 we can adjust the position of the overlapped laser paths. After PBS3, reflected component of path1 and transmitted component of path2 is chosen. This consists of two spatially separated laser paths with each path having overlapped trapping and tracking light. Mirrors M1 and M2 with the help of mirror M8 are used to steer the light into the objective entrance pupil.

The microscopic beads are trapped in dual optical tweezer the similar way to that of trapping in single optical tweezer. Simultaneous trapping of beads in both the traps is achieved. The two traps can be independently steered using the mirrors M6 and M7.

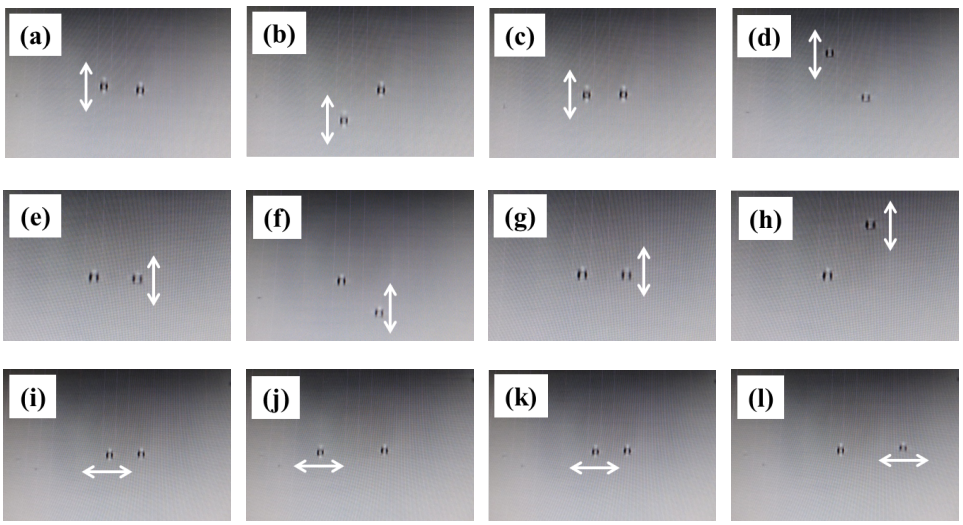


Figure 3.8: Shows the independent steer of the dual optical tweezer traps. The spheres are trapped microscopic beads. (a), (b), (c), (d) shows the vertical displacement of the trap on the left-hand side. (e), (f), (g), (h) shows the vertical displacement of the trap on the right-hand side. (i), (j), (k), (l) shows the horizontal displacement of the trap.

## 3.5 Stiffness calculation of dual optical tweezer

Power spectral density method is used to find the stiffness of dual optical tweezer. The forward scattered light now has the information of both the traps. The difference in the polarization of the light in both the traps is used to separate the two tracking lights. The reflected component of path1 and transmitted component of path2 has polarizations perpendicular to each other. The polarizing beam splitter (PBS2) reflects path1 light and transmits path2 light. A dichroic mirror (DM2) is placed between PBS2 and microscope lamp reflects the path2 light and transmits the microscope bright light. The quadrant photodiode mounted on an XYZ translator is used to monitor the bead movement. Using the translator, the single QPD is moved vertically to monitor the bead movements in both the traps separately. The filter (F1) in front of the QPD ensures transmission of only tracking light.

Beads are trapped simultaneously in both the traps and QPD is used to monitor position fluctuation in a single trap. As mentioned earlier spectrum analyzer is used to get the power spectral density of the Brownian motion of trapped beads. From PSD, corner frequency is obtained from which the trap stiffness is calculated.

## 3.6 Construction of fluorescence microscope

Imaging the microtubules is one of the essential steps in studying mix-molecular-motor assays. Microtubules are very thin structures with diameter of the order of 10's of nm which makes it difficult to image using microscope bright light. To overcome this problem, they are generally tagged using fluorescent dyes and imaged using fluorescence microscopy. A fluorescent microscope is being built using a bright mercury lamp (Olympus, model number: U-LH100HG) that illuminates the sample chamber from the bottom. The lamp is placed in the reflection path of the dichroic mirror (DM1) present near the entry port of the microscope. The forward scattered light is reflected using a 50-50 beam splitter and is viewed using a CMOS camera (Thorlabs, model number: DCC1545M-GL). The figure 3.9(b) shows the optical layout of the fluorescence microscope. Emission and excitation filters are decided by the type of dye used for tagging microtubules.

A sample containing mixture of 2 $\mu$m non-fluorescent beads (Bangs Laboratories, model number: NT17N) and 100 nm fluorescent beads (TetraSpeck, model number: T7279) are imaged using the fluorescent microscope setup. The 100 nm beads can fluoresce at four different colors. Tetramethylrhodamine dye with excitation and emission peaks at 550 nm and 575 nm respectively is used to tag the microtubules. The 100 nm beads also fluoresce orange in the similar range and the respective excitation and emission peaks are 540 nm and 560 nm. The excitation and emission spectra of the tetramethyl rhodamine dye and tetraspeck beads in orange are given in the figures 3.10(a) and 3.10(b). To check fluorescence, the following filters are used.

- Excitation filter (Chroma technology, model number: D540/20m)

  Transmission wavelength: 530 - 550 nm

- Emission filter (Nikon, model number: BA590)

  Transmission wavelength: above 590 nm

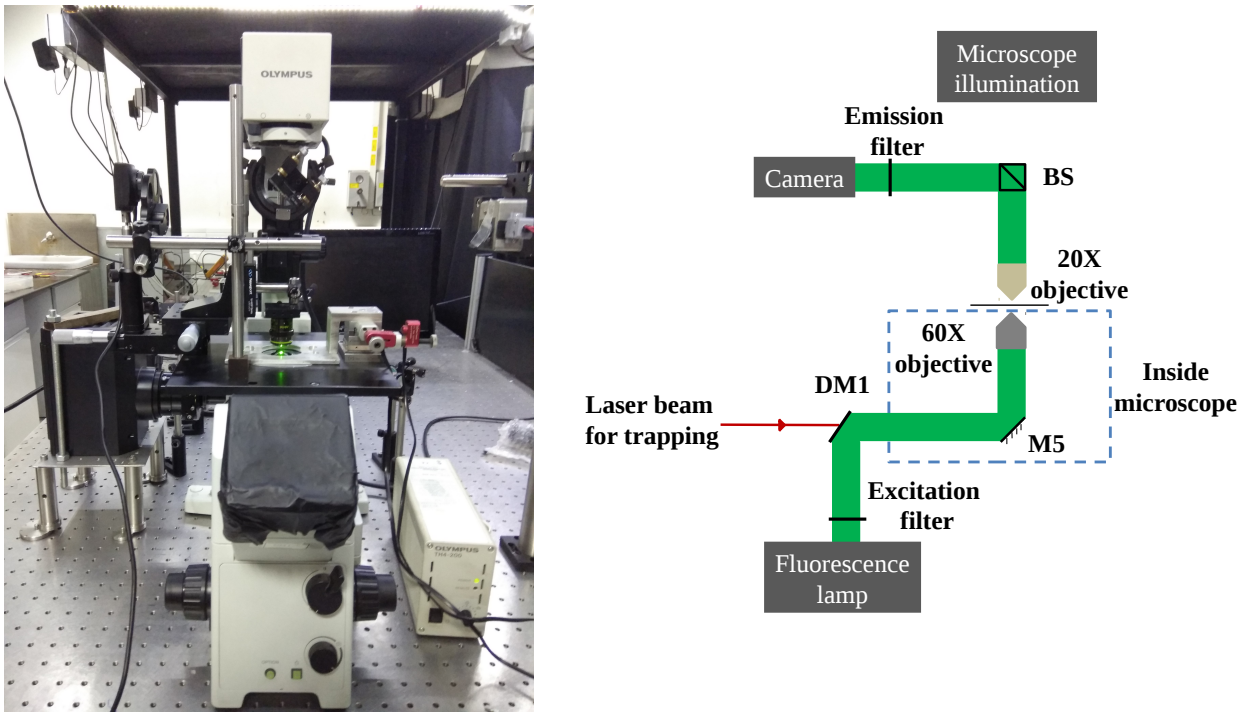


Figure 3.9: **Left panel**: Fluorescence microscopy setup. **Right panel**: Fluorescence microscopy optical layout.

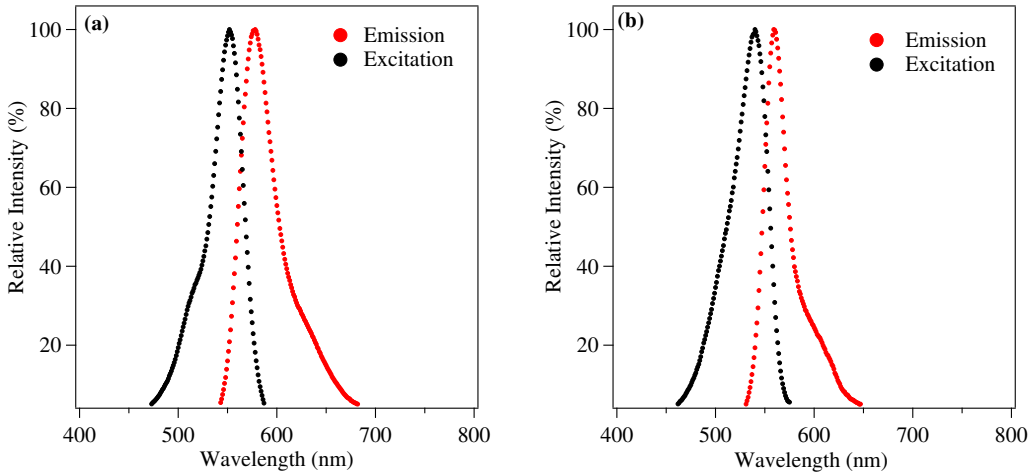


Figure 3.10: (a) Spectra for tetramethyl rhodamine dye. (b) Spectra for tetraspeck beads in orange.

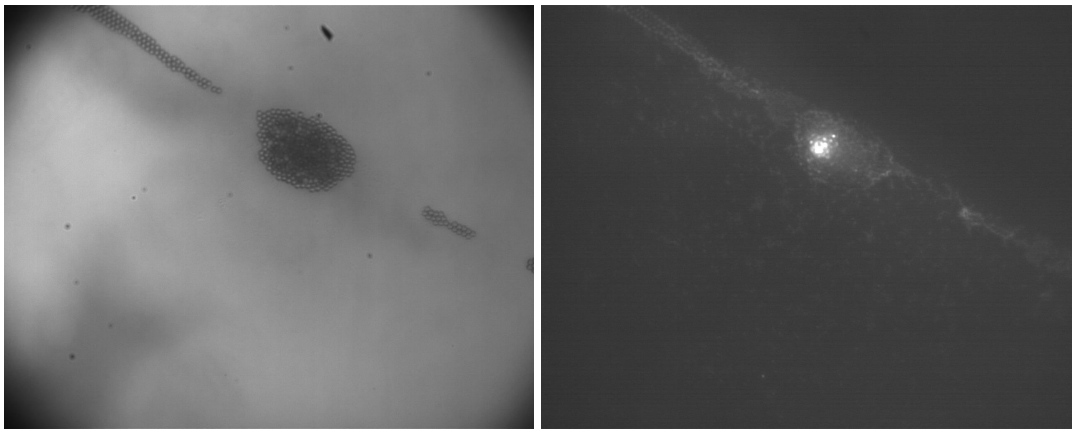

Figure 3.11: (a) Bright field image taken in the lab microscope. (b) Fluorescence image taken in the lab microscope.

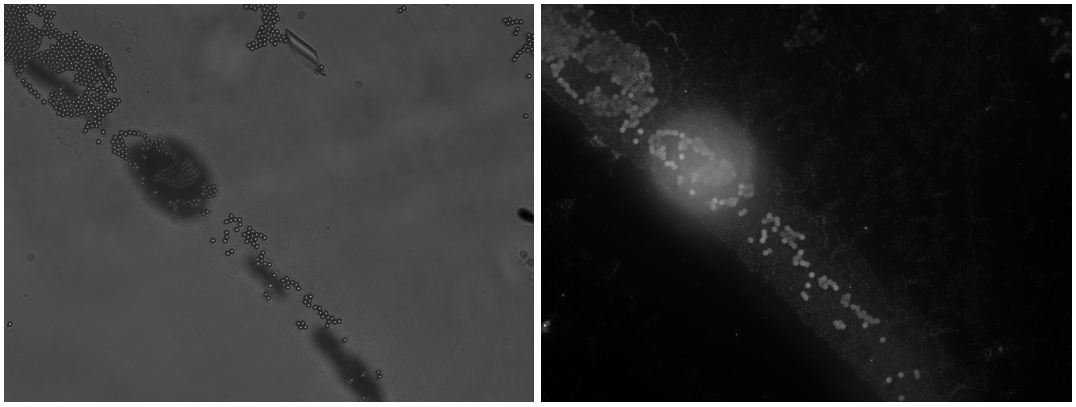

Figure 3.12: (a) Bright field image taken in the commercial microscope. (b) Fluorescence image taken in the commercial microscope.

The sample is imaged using the home made fluorescence microscope and commercial microscope (Zeiss AxioImager Z1). The images taken from our home made setup are given in figures 3.11(a) and 3.11(b), the image taken from commercial system are given in figure 3.12(a) and 3.12(b). We can see smaller particles in the fluorescent images that are not present in the bright field images, which corresponds to the 100 nm tetraspeck fluorescent beads. On comparison of these images, we can say that our system is up-to the mark for performing experiments with mix-molecular-motor assays.

# Chapter 4

# Results

## 4.1 Single optical tweezer

As mentioned earlier power spectral density method is used to find the trap stiffness of optical tweezer.

$$S_x(\omega) = \frac{k_B T}{\gamma \pi^2 (f^2 + f_c^2)} \tag{4.1}$$

This follows Lorentzian distribution and is modeled using the following equation

$$y = y_0 + \frac{A}{(x - x_0)^2 + B} \tag{4.2}$$

where $x_0$ and $y_0$ are constants and kept at zero in present calculation. Comparing the equations 4.1 and 4.2 gives corner frequency $f_c = \sqrt{B}$. The trap stiffness is given by

$$k_{trap} = 2\pi f_c \gamma \tag{4.3}$$

here $f_c$ is corner frequency, $\gamma = 6\pi\eta a$ is friction coefficient, $a$ is the radius of the trapped bead. The friction coefficient can be found out from the value of $\eta$, which is the fluid viscosity. The viscosity of water at 298 K is $8.90 \times 10^{-4}$ Pa-s.

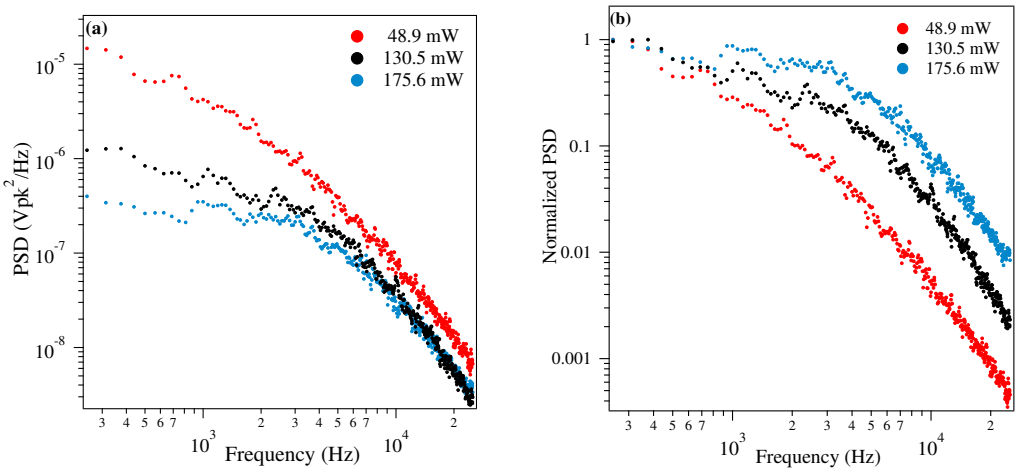


Figure 4.1: (a) Power spectral density vs frequency for 1 $\mu$m beads. (b) Normalized power spectral density vs frequency for 1 $\mu$m beads.

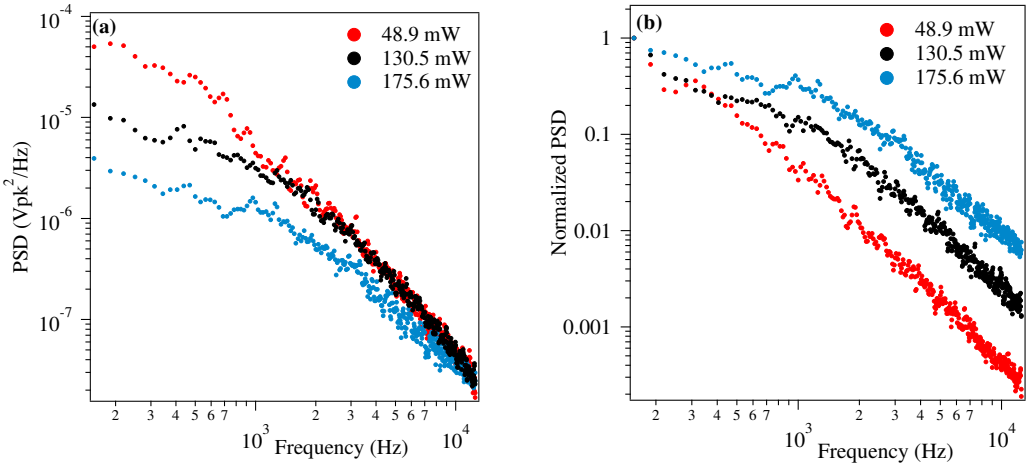


Figure 4.2: (a) Power spectral density vs frequency for 2 $\mu$m beads. (b) Normalized power spectral density vs frequency for 2 $\mu$m beads.

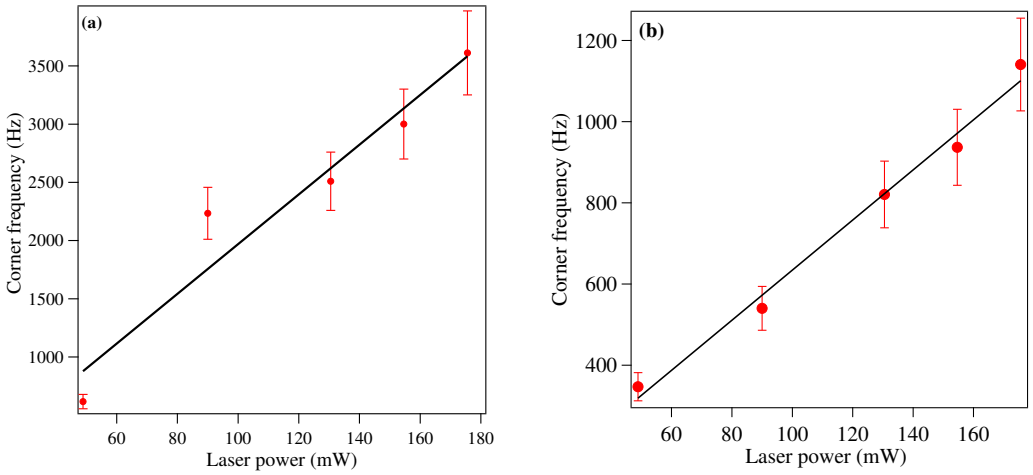


Figure 4.3: (a) Corner frequency vs laser power for 1 micron bead. (b) Corner frequency vs laser power for 2 micron bead.

Beads of both 1 $\mu$m and 2 $\mu$m are trapped to find how the trap stiffness changes with the bead size. PSD data is acquired for both kind of beads at different trapping powers as shown in figure 4.1(a) and 4.2(a). The trapping power is the power measured after the 60X objective where trapping is realized. The acquisition time of spectrum analyzer is set to 15.6 ms with a frequency span of 0 - 25 KHz for 1 $\mu$m bead. For 2 $\mu$m sized beads, the acquisition time is 31.3 ms with frequency span of 0 - 12.8 KHz. All the signals are acquired after averaging over 30 instants.

The normalized power spectral density graphs of 1 $\mu$m and 2 $\mu$m beads are given in the figures 4.1(b) and 4.2(b) respectively. Both the graphs consist of a constant region which represents the suppressed motion of the trapped bead. After a particular frequency, the graphs show fast decay representing the free diffusion. The corner frequency is measured from power spectral density by fitting it with Lorentzian. The graphs 4.3(a) and 4.3(b) shows the experimental values of corner frequencies obtained. We can see a linear increase in the corner frequencies with trapping laser power. The trap stiffness is calculated from the obtained value of corner frequency. The figures 4.4(a) and 4.4(b) shows linear relationship between the trap stiffness and the trapping laser power.

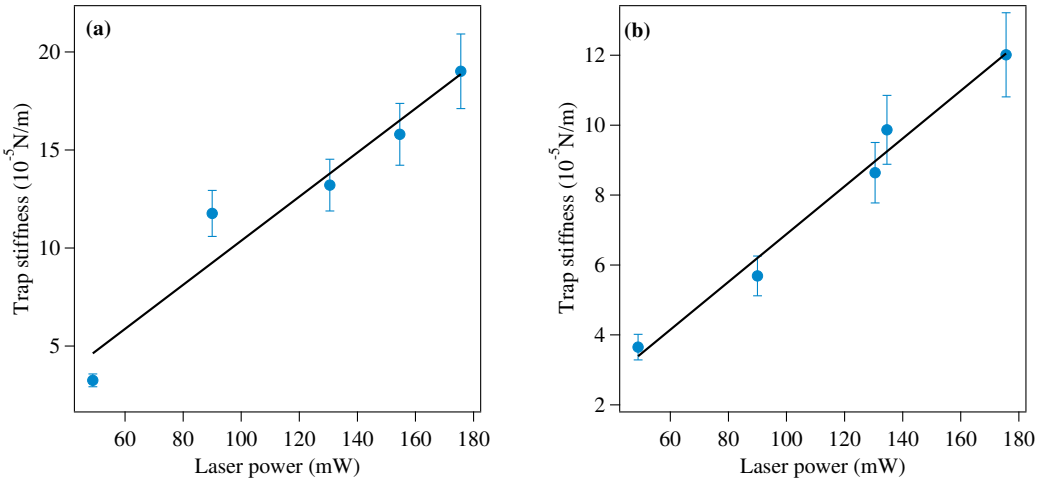


Figure 4.4: (a) Trap stiffness vs laser power for 1 micron bead. (b) Trap stiffness vs laser power for 2 micron bead.

An error bar of $\pm$ 10% is included in all the graphs. The Lorentzian fitting of the power spectral densities also gave a variation about $\pm$ 10% standard deviation in the value of B. Hence the same amount of variation can be expected in the calculated value of corner frequency. The bead manufacturer data sheet specifies a variation of $\pm$ 10% in the sizes of both 1 $\mu$m and 2 $\mu$m beads. Since the trap stiffness is linearly proportional to the bead radius, $\pm$ 10% variation can be expected in the value of trap stiffness also.

## 4.2 Dual optical tweezer

The dual optical tweezer is also calibrated using the PSD method. 2 $\mu$m beads are trapped simultaneously in both the traps. Since there is only one QPD, the dual trap calibration is performed by trapping beads in both the traps and finding the PSD of Brownian motion of trapped bead in a single trap at one instant. Henceforth the individual traps in dual optical tweezer are named as 'first trap' and 'second trap'. The spectrum analyzer is set to 31.3 ms acquisition time with frequency span of 0 - 12.8 KHz. All the signals are acquired after averaging over 30 instants.

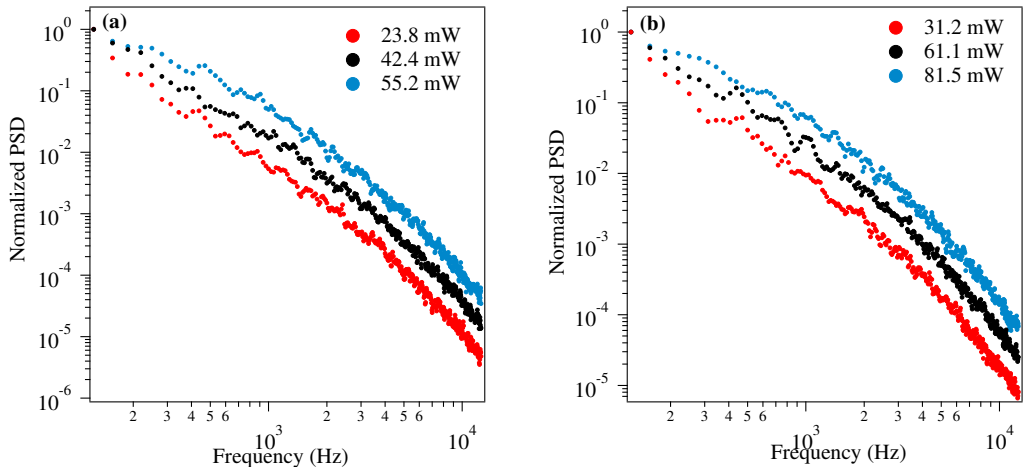


Figure 4.5: (a) Normalized power spectral density vs frequency for first trap. (b) Normalized power spectral density vs frequency for second trap

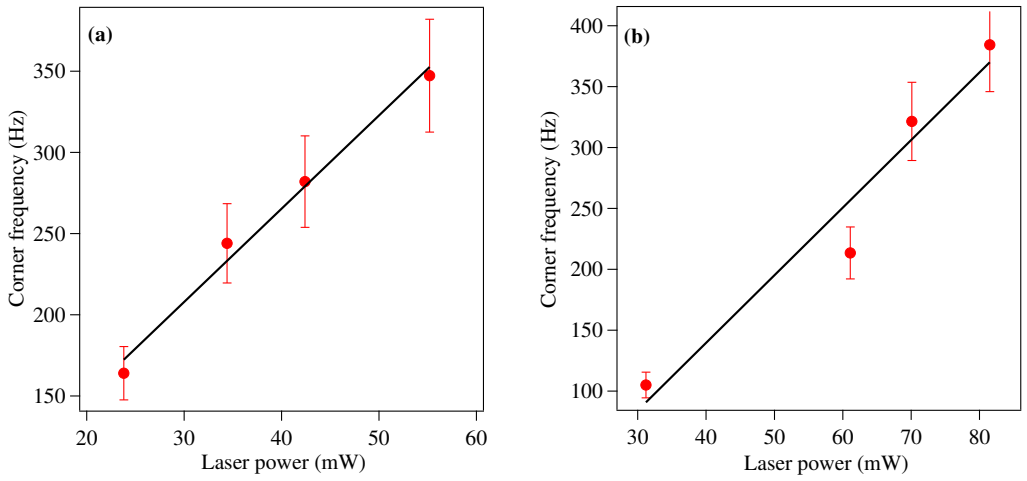


Figure 4.6: (a) Corner frequency vs laser power for first trap. (b) Corner frequency vs laser power for the second trap

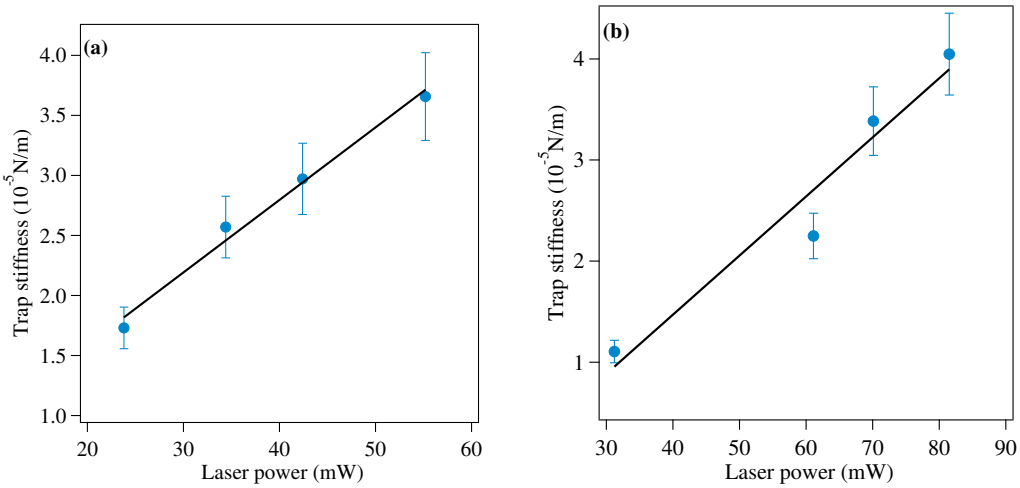


Figure 4.7: (a) Trap stiffness vs laser power for first trap. (b) Trap stiffness vs laser power for the second trap.

The normalized PSD graphs of 2 $\mu$m beads in two different traps of dual optical tweezer are given in the figures 4.5(a) and 4.5(b). The figures 4.6(a) and 4.6(b) shows the linear relationship between the corner frequency and the trapping laser power for dual optical tweezer. In the figures 4.7(a) and 4.7(b), the trap stiffness of first and second trap in dual optical tweezer with trapping laser power is plotted. They also show linear relationship.

# Chapter 5

# Discussion

In the earlier chapter we saw calibration of both single and dual optical tweezer. The corner frequency values for 2 $\mu$m polystyrene beads from the experiment is compared with the literature value reported by Astrid van der Horst *et al.* [33]. The comparison is shown in figure 5.1. Both the experimental setup used 60X water immersion objective. They used polystyrene beads sized 2.1 $\mu$m with a variation of $\pm$ 10% in size. Both the experimental value and the literature value matches considerably within the error bar.

Another graph is plotted by taking the trap stiffness values of individual traps of dual optical tweezer along with the values for single optical tweezer. The plot is shown in the figure 5.2. We can see that the dual optical tweezer with two traps along with single optical tweezer follows a linear relationship between the trap stiffness and the trapping laser power. Since the dual tweezer is experimentally derived from single optical tweezer using a polarizing beam splitter, it is just an extension of the single optical tweezer.

One of the major difficulty faced during the experiment was the accumulation of multiple beads in a single trap. The 60X objective with N.A. of 1.2 used in the experiment resulted in a larger beam waist at the focus of the objective. This caused more than one bead to be trapped in a single trap. This created problems in the calibration part since the quadrant photodiode gets

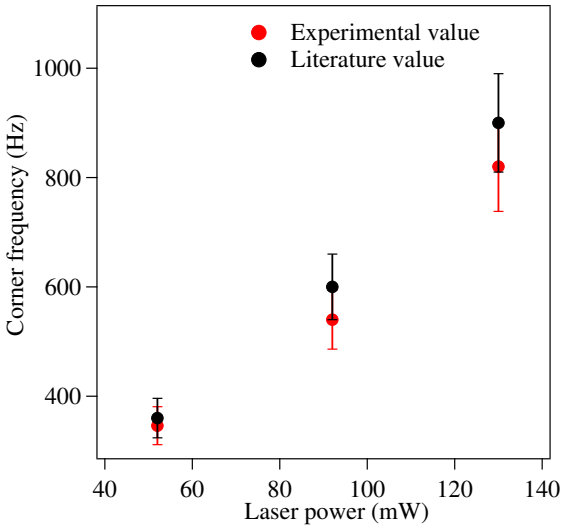


Figure 5.1: Comparison of experimental corner frequency values for 2 $\mu$m bead with literature value

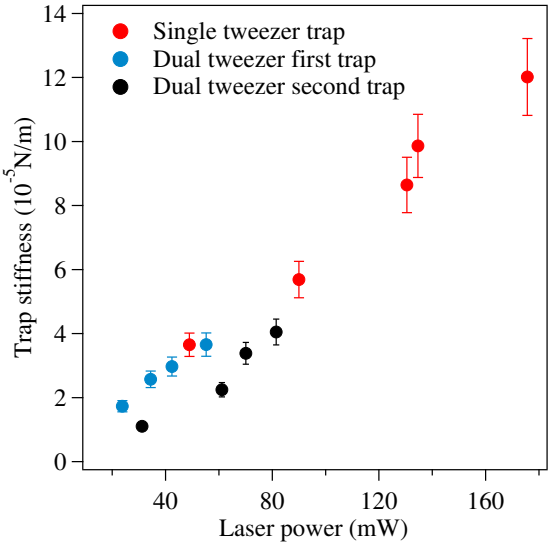


Figure 5.2: Comparison of experimental corner frequency values for 2 $\mu$m bead with literature value

information of the movement of more than one trapped bead. To circumvent this, a high N.A. oil immersion objective can be used to ensure single bead trapping.

## 5.1 Future plans

The immediate plan is to combine fluorescence microscopy with the dual optical tweezer system. This would help to achieve simultaneous trapping and fluorescence imaging. Once it's achieved, we would move on to perform the real experiments using mix-molecular-motor assays.

# Bibliography


[1] J. Kepler. *De cometis libelli tres*. 1619.

[2] J.C. Maxwell. *On Physical Lines of Force*. Nineteenth Century Collections Online (NCCO): Science, Technology, and Medicine: 1780-1925. 1861.

[3] Peter Lebedew. Untersuchungen über die druckkräfte des lichtes. *Annalen der Physik*, 311(11):433–458, 1901.

[4] Ernest Fox Nichols and Gordon Ferrie Hull. The pressure due to radiation. In *Proceedings of the American Academy of Arts and Sciences*, volume 38, pages 559–599. JSTOR, 1903.

[5] Arthur Ashkin. Acceleration and trapping of particles by radiation pressure. *Physical review letters*, 24(4):156, 1970.

[6] TH Maiman. Speech by dr. theodore h. maiman, hughes aircraft company. at a Press Conference at the Hotel Delmonico, New York, 1960.

[7] Arthur Ashkin, James M Dziedzic, JE Bjorkholm, and Steven Chu. Observation of a single-beam gradient force optical trap for dielectric particles. *Optics letters*, 11(5):288–290, 1986.

[8] Arthur Ashkin and James M Dziedzic. Optical trapping and manipulation of viruses and bacteria. *Science*, 235(4795):1517–1520, 1987.

[9] Karel Svoboda and Steven M Block. Biological applications of optical forces. *Annual review of biophysics and biomolecular structure*, 23(1):247–285, 1994.

[10] David G Grier. Optical tweezers in colloid and interface science. *Current opinion in colloid & interface science*, 2(3):264–270, 1997.

[11] Nobutaka Hirokawa. Kinesin and dynein superfamily proteins and the mechanism of organelle transport. *Science*, 279(5350):519–526, 1998.

[12] David D Hackney. The kinetic cycles of myosin, kinesin, and dynein. *Annual review of physiology*, 58(1):731–750, 1996.

[13] Karel Svoboda, Christoph F Schmidt, Bruce J Schnapp, and Steven M Block. Direct observation of kinesin stepping by optical trapping interferometry. *Nature*, 365(6448):721, 1993.

[14] Zhaohui Wang, Shahid Khan, and Michael P Sheetz. Single cytoplasmic dynein molecule movements: characterization and comparison with kinesin. *Biophysical journal*, 69(5):2011–2023, 1995.

[15] Junya Ikuta, Nagendra K Kamisetty, Hirofumi Shintaku, Hidetoshi Kotera, Takahide Kon, and Ryuji Yokokawa. Tug-of-war of microtubule filaments at the boundary of a kinesin- and dynein-patterned surface. *Scientific reports*, 4:5281, 2014.

[16] Benjamin H Blehm, Trina A Schroer, Kathleen M Trybus, Yann R Chemla, and Paul R Selvin. In vivo optical trapping indicates kinesins stall force is reduced by dynein during intracellular transport. *Proceedings of the National Academy of Sciences*, 110(9):3381–3386, 2013.

[17] William O Hancock. Bidirectional cargo transport: moving beyond tug of war. *Nature reviews Molecular cell biology*, 15(9):615, 2014.

[18] Kazuya Suzuki, Makito Miyazaki, Jun Takagi, Takeshi Itabashi, and Shinichi Ishiwata. Spatial confinement of active microtubule networks induces large-scale rotational cytoplasmic flow. *Proceedings of the National Academy of Sciences*, page 201616001, 2017.

[19] Vinay Swaminathan, Joseph Mathew Kalappurakkal, Shalin B Mehta, Pontus Nordenfelt, Travis I Moore, Nobuyasu Koga, David A Baker, Rudolf Oldenbourg, Tomomi Tani, Satyajit Mayor, et al. Actin retrograde flow actively aligns and orients ligand-engaged integrins in focal adhesions. *Proceedings of the National Academy of Sciences*, 114(40):10648–10653, 2017.

[20] Todd Fallesen, Johanna Roostalu, Christian Duellberg, Gunnar Pruessner, and Thomas Surrey. Ensembles of bidirectional kinesin cin8 produce additive forces in both directions of movement. *Biophysical journal*, 113(9):2055–2067, 2017.

[21] Keir C Neuman and Steven M Block. Optical trapping. *Review of scientific instruments*, 75(9):2787–2809, 2004.

[22] Yasuhiro Harada and Toshimitsu Asakura. Radiation forces on a dielectric sphere in the rayleigh scattering regime. *Optics communications*, 124(5-6):529–541, 1996.

[23] Arthur Ashkin. Forces of a single-beam gradient laser trap on a dielectric sphere in the ray optics regime. *Biophysical journal*, 61(2):569–582, 1992.

[24] Wikipedia article on optical tweezer.

[25] Albert Einstein. On the motion of small particles suspended in liquids at rest required by the molecular-kinetic theory of heat. *Annalen der physik*, 17:549–560, 1905.

[26] Kirstine Berg-Sørensen, Erwin JG Peterman, Tom Weber, Christoph F Schmidt, and Henrik Flyvbjerg. Power spectrum analysis for optical tweezers. ii: Laser wavelength dependence of parasitic filtering, and how to achieve high bandwidth. *Review of scientific instruments*, 77(6):063106, 2006.

[27] George E Uhlenbeck and Leonard S Ornstein. On the theory of the brownian motion. *Physical review*, 36(5):823, 1930.

[28] Kirstine Berg-Sørensen and Henrik Flyvbjerg. Power spectrum analysis for optical tweezers. *Review of Scientific Instruments*, 75(3):594–612, 2004.

[29] Graham M Gibson, Jonathan Leach, Stephen Keen, Amanda J Wright, and Miles J Padgett. Measuring the accuracy of particle position and force in optical tweezers using high-speed video microscopy. *Optics Express*, 16(19):14561–14570, 2008.

[30] Frederick Gittes and Christoph F Schmidt. Signals and noise in micromechanical measurements. In *Methods in cell biology*, volume 55, pages 129–156. Elsevier, 1997.

[31] Arpit Yati. Towards the experimental realization of directed transport in equibrium. *Master's thesis*, 2011.

[32] A Pralle, M Prummer, Ernst-Ludwig Florin, EHK Stelzer, JKH Hörber, et al. Three-dimensional high-resolution particle tracking for optical tweezers by forward scattered light. *Microscopy research and technique*, 44(5):378–386, 1999.

[33] Astrid van der Horst and Nancy R Forde. Power spectral analysis for optical trap stiffness calibration from high-speed camera position detection with limited bandwidth. *Optics express*, 18(8):7670–7677, 2010.